Emerging Microbes & Infections
2025, VOL. 14, 2466695 (19 pages)
https://doi.org/10.1080/22221751.2025.2466695

GNLY+CD8+ T cells bridge premature aging and persistent inflammation in people living with HIV

Hui-Fang Wang[a,b*], Chao Zhang[b*], Li-Ping Zhang[b*], Cheng Zhen[b], Liang Zhao[b], Hui-Huang Huang[b], Bao-Peng Yang[b], Si-Yuan Chen[b], Wei-Zhe Li[b], Ming-Ju Zhou[b], Qian-Xi Guo[b], Xia Li[b], Bai-Lu Yin[b], Fang Sun[b], Ji-Yuan Zhang[b‡], Zhixin Zhang[c], Fu-Sheng Wang[b] and Qing-Lei Zeng[a]

[a]Department of Infectious Diseases and Hepatology, The First Affiliated Hospital of Zhengzhou University, Zhengzhou, People's Republic of China; [b]Senior Department of Infectious Diseases, The Fifth Medical Center of Chinese PLA General Hospital, Beijing, People's Republic of China; [c]Department of Technology, Chengdu ExAb Biotechnology LTD, Chengdu, People's Republic of China

ABSTRACT

People living with HIV (PLWH) exhibit accelerated aging, characterized by systemic inflammation, termed "inflammaging." While T-cell expansion is prevalent in PLWH, its connection to inflammaging remains unclear. In this study, we analyzed the TCRβ repertoire of 257 healthy controls (HC) and 228 PLWH, revealing pronounced T cell clonal expansion in PLWH. The expansion was only partially reversed following antiretroviral therapy (ART) and closely associated with ART duration, CD4+ T and CD8+ T cell counts and the CD4/CD8 ratio. TCR-based age modeling showed a continuous accelerated trajectory of aging in PLWH, especially in younger individuals, in stark contrast to the nonlinear aging acceleration pattern seen in HC. Furthermore, using single-cell RNA combined TCR sequencing and in vitro experiments, we identified GNLY+CD8+ T cells as the primary population driving clonal expansion and maintenance in PLWH. These cells are characterized by high cytotoxicity and low exhaustion and are activated by interleukin-15 (IL-15) in vitro. Notably, GNLY+CD8+ T cells predominantly express the pro-inflammatory 15 kDa form of granulysin(GNLY). The supernatant from IL-15-stimulated CD8+ T cells induces monocytes to secrete inflammatory factors and disrupts the integrity of intestinal epithelial cells, which can be partially restored by the anti-GNLY antibodies. These findings identify GNLY+CD8+ T cells as the central drivers of persistent clonal expansion, highlighting their crucial role for mitigating inflammaging in PLWH.

ARTICLE HISTORY Received 6 November 2024; Revised 16 January 2025; Accepted 9 February 2025

KEYWORDS HIV; TCR repertoire; GNLY+CD8+ T cells; clonal expansion; inflammaging

Introduction

HIV/AIDS is characterized by disrupted immune homeostasis and decreased immune surveillance, leading to opportunistic infections, autoimmune diseases and malignancies [1]. Antiretroviral therapy (ART) significantly prevents AIDS-related complications and prolongs life in people living with HIV (PLWH) [2]. However, healthspan, as opposed to lifespan, remains significantly shorter for PLWH, even for those who started ART with CD4+ T cell counts above 500 cells/ul, compared to uninfected adults [3]. The primary concern is the onset of multiple age-related morbidities [3], contributed by chronic, systemic inflammation that increases with age, a process termed "inflammaging" [4,5]. In PLWH, inflammaging is reported to coexist with many factors, such as ongoing, low levels of HIV replication, ART-induced mitochondrial toxicities, other co-infections and dysbiosis [6,7]. However, the mechanisms that lead to exaggerated inflammaging in PLWH are not well understood, and there is also a lack of appropriate therapeutic strategies.

Abnormal expansion of CD8+ T cells takes place during HIV-1 infection [8–10], which cannot be restored even after more than a decade of ART [11,12]. The idiosyncratic and persistent expansion of CD8+ T cells [12–14] is associated with T cell senescence, activation, dysfunction and chronic inflammation [14,15], and has been linked to poor aging in PLWH [10,16,17]. Additionally, the disturbances in T cell clonal expansion are characteristic of age-related changes [18] and have become a key indicator for assessing biological age for healthy individuals [19]. Moreover, clonally expanded CD8+ T cells are a significant source of various cytokines, including tumor necrosis factor (TNF)-α and interferons (IFN)-γ [20,21], which

CONTACT Zhixin Zhang jason_zhang2011@hotmail.com; Fu-Sheng Wang fswang302@163.com; Qing-Lei Zeng zengqinglei2009@163.com
*Hui-Fang Wang, Chao Zhang and Li-Ping Zhang contributed to the work equally.
‡We would like to dedicate this paper to Ji-Yuan Zhang, who unfortunately passed away just before the paper was submitted for publication. Ji-Yuan Zhang played an essential role in this research described here and he is greatly missed.
Supplemental data for this article can be accessed online at https://doi.org/10.1080/22221751.2025.2466695.

play a crucial role in inflammation. However, the specific phenotypic characteristics of clonally expanded CD8+ T cells in PLWH remain unclear, and the link between such disturbed T cell pools and inflammaging requires further investigation.

To conduct a comprehensive and unbiased analysis of disrupted T cells in PLWH, we integrated bulk TCR and single-cell RNA combined TCR sequencing to delineate dynamic changes of TCR repertoire across different stages of PLWH. We identified age-related granulysin (GNLY)+CD8+ T cells as the primary subpopulation for clonal maintenance and expansion. GNLY+CD8+ T cells exhibit high cytotoxicity and low exhaustion markers, and are expanded by interleukin-15 (IL-15) in vitro. The supernatant derived from IL-15-stimulated CD8+ T cells demonstrates pro-inflammatory effects on monocytes and disrupts the integrity of intestinal epithelial cells. This disruption can be partially restored by the application of anti-GNLY antibodies. Thus, these findings underscore the crucial role of expanded GNLY+CD8+ T cells in driving exacerbated inflammaging in PLWH.

Materials and methods

Clinical samples and characteristics

Two cohorts of people living with HIV (PLWH) were recruited at the Fifth Medical Center of Chinese PLA General Hospital in Beijing, China from January 2021 to March 2023. The inclusion criteria comprised being over 18 years old and having a confirmed HIV-1 positive status. Exclusion criteria included pregnancy and breastfeeding, as well as co-infection with hepatitis B or hepatitis C viruses, tuberculosis and other opportunistic infections [22].

For TCRβ gene sequencing, a cross-sectional set of 228 PLWH was enrolled in this study. The age – and sex-matched 257 HC were obtained from the healthy TCRβ database at Chengdu ExAb Biotechnology [23]. Further details on the characteristics of each group can be found in supplementary Table 1. An additional cohort of 10 HC, 18 TP, 23 IR and 23 INR was used for flow analysis to validate the sequencing results. Detailed clinical information is provided in supplementary Table 2.

Sample collection and cell isolation

Samples were collected after participants signed informed consent. Approximately 2 ml of fresh peripheral blood was collected via venipuncture with lavender top tubes using ethylene diamine tetraacetic acid (EDTA) as an anticoagulant. The plasma obtained after centrifugation was stored at – 80°C for further analysis. Peripheral blood mononuclear cells (PBMCs) were isolated by Ficoll-Hypaque density gradient centrifugation, and the cell number was counted with a hemocytometer under a microscope.

TCRβ gene sequencing and analysis

Total RNA purification and two rounds of polymerase chain reaction (PCR) amplification of the TCRβ gene were performed according to a previously described method [23]. Briefly, total RNA was extracted using Trizol reagent (Invitrogen, USA) as per the manufacturer's instructions, and its concentration was quantified using a NanoDrop 2000 spectrophotometer (Life Technologies, USA). The extracted RNA served as a template for the first round of reverse transcription-PCR (RT–PCR) amplification of the TCRβ gene using the QIAGEN One-Step RT–PCR kit (QIAGEN, USA), with TRTmix and Vbmix primers used, which are 1:1 mixtures designed based on the functional human T-cell receptor β constant (TRBC) and β variable (TRBV) alleles (Supplementary Table 3,4). RT–PCR conditions were as follows: reverse transcription, 50°C, 30 min; PCR activation, 95°C, 15 min; and then, 20 cycles of reactions, 95°C, 30 s; 58°C, 30 s; and 72°C, 30 s. The product from first-round RT–PCR was subsequently utilized as a template for a second round of PCR amplification employing Vbmix primers and barcode-containing hTCRCbBCX primers (Supplementary Table 5) to enhance the amplification of the TCRβ gene. The PCR conditions were as follows: activation, 95°C, 10 min and 20 cycles of reactions, 95°C, 30 s; 58°C, 30 s; and 72°C, 30 s. The PCR products of the two rounds were ultimately purified with the DNA fragment purification kit (BioMagbeads, China).

Sequencing libraries were assembled utilizing the Thermal-Fisher Ion Plus Fragment Library Kit (Thermo Fisher Scientific, USA), Ion Xpress Barcode Adapter 1-16Kit (Thermo Fisher Scientific, USA) and Agencourt AMPure XP (Thermo Fisher Scientific, USA) according to the manufacturer's instruction. Automatic template preparation and chip loading were performed on the Thermal-Fisher Ion Chef system using the Ion 520/530 ExT-Chef-4rxns&4Init NEW-For600 bp (Thermo Fisher Scientific, USA). Subsequently, the Ion S5 system was utilized for sequencing the TCRβ variable region with the Ion 530 Chip Kit (Thermo Fisher Scientific, USA).

After high-throughput sequencing, each sample was exported as a separate FASTA file based on the barcode. Vβ, Jβ genes, and CDR3 amino acid sequences were analyzed using a local IgBLAST program. A "functional" TCRβ sequence is a V-D-J junction that produces a productive translation of the TCRβ peptide with non-empty CDR3. To unify the number of clones for comparison, 30,000 functional TCRβ sequences were randomly selected from each sample for all the following repertoire analyses.

Clonality and diversity indices of TCRβ repertoire

To accurately quantify clonality, considering both the types and proportions of clonal expansion, we initially defined large and big clones as unique TCRβ CDR3 clonotypes accounting for >1% and 0.1–1% of 30,000 functional randomly selected sequences, respectively. In addition, we combined the percentages represented by the top 10 and 20 clones to evaluate the clonality of the TCRβ repertoire.

To assess diversity, we employed four mathematical indices: Richness, Gini coefficient, Shannon entropy, and D50. Richness measures the number of unique clonotypes, while the Gini coefficient quantifies the evenness of distribution. Shannon entropy, which integrates both clonotype richness and evenness, provides a comprehensive measure of diversity but is particularly sensitive to increases in low-frequency clones. In contrast, D50 is a straightforward diversity metric that focuses on dominant clones within TCR repertoire, thereby minimizing the influence of low-frequency clones on the results [24,25].

ScRNA coupled scTCR sequencing

The raw scRNA-seq (10× Genomics) and scTCR-seq data of CD4 + T and CD8 + T cells were obtained from the Genome Sequence Archive of the Beijing Institute of Genomics Data Center, Chinese Academy of Sciences [http://bigd.big.ac.cn/gsa-human, accession code: HRA000190, uploaded], which was published by our group [2]. The Cell Ranger toolkit V.3.1.0 was applied to align reads and generate the gene-cell unique molecular identifier (UMI) matrix against the human reference genome GRCh38 provided by 10× Genomics. Then the R software (v.3.5.3) with the Seurat package (v.3.0.0) was used for data quality control. We quantified the number of genes and UMIs and kept high-quality cells with more than 1000 UMIs, more than 500 genes detected and no more than 10% of mitochondrial gene counts. The Scrublet package (v.0.2.3) in Python (v.3.9.7) was applied to each dataset to detect potential doublets with an expected doublet rate of 6%, and the cells with scores exceeding 0.5 were considered doublets and filtered out. After these cells, the gene expression matrices were normalized by NormalizeData function in Seurat, and then processed for dimension reduction, batch effect correction and unsupervised clustering.

Polynomial regression and sliding window analysis

We used the Stats R package (version 4.4.1) for polynomial regression analysis, applying the poly (x, degree = 3) function to perform polynomial expansion on the independent indicators, and then fitting the model using lm(y ~ poly(x, degree)). The sliding window analysis was performed with DEswan R package (version 0.1.0), 8 indicators were respectively subjected to the sliding window analysis with a window of 5 years by comparing groups in parcels of 2 years.

Antibodies and flow cytometry

Anti–CD3-BUV395 (clone HIT3a), Anti–CD3-BV605 (clone SK7), anti–CD8-BUV496 (clone SK1), anti–CD8-BUV737 (clone SK1), anti–CD56-BB700 (clone B159), anti–Granzyme B-BV510 (clone GB11), anti–Granulysin-AF488 (clone RB1), anti–HLA-DR-Percp Cy5.5 (clone L243), anti–CCR7–BUV395 (clone 3D12), anti–CD27–BUV496 (clone M-T271), anti-CD28-Percp Cy5.5 (clone CD28.2), anti–PD-1-BV650 (clone NAT105), anti-CD57-BV421 (clone NK-1) and anti-CD45RA-PE/CY7 (clone HI100) were purchased from BD Bioscience. anti–HLA-DR-BV421 (clone L243), Anti–CD56-BV711 (clone 5.1H11), anti–NKG2D-BV785 (clone 1D11), anti–KLRG1-PE (clone 14C2A07), anti–CD38-PE/CY7 (clone HB-7), anti–T-bet-BV785 (clone 4B10), anti–PD-1-BV711 (clone NAT105) and anti–Granulysin-PE/CY7 (clone DH2) were purchased from BioLegend. Anti–Perforin-PE/CY7 (clone dG9) and anti–EOMES-PE (clone WD1928) were purchased from Invitrogen and Thermo Fisher Scientific.

For phenotypical staining, cryopreserved PBMCs were thawed in a complete medium and then stained extracellularly using surface antibodies for 30 minutes at 4°C. The cells were subsequently washed with FACS buffer. After washing, the cells were permeabilized and fixed using the eBioscience™ Foxp3 Permeabilization/Fixation Kit (Invitrogen) according to the manufacturer's instructions. The cells were then incubated for 30–50 minutes at 4°C with antibodies for intracellular staining. Samples were acquired on a FACS Canto II flow cytometer (BD Biosciences) and analyzed with FlowJo software v.10.

Immunoblotting

To distinguish the different expression levels of 9 and 15 kDa GNLY, CD8 + T cells were first isolated from fresh PBMC using CD8 positive magnetic selection (Miltenyi Biotech, Germany). Non-magnetically labeled cells were then subjected to the NK cell negative magnetic selection (Miltenyi Biotech, Germany) isolation kit to obtain negative enriched NK cells and other cells captured by magnetic beads. Total proteins were extracted with RIPA buffer supplemented with 1× protease and phosphatase inhibitor cocktail

(Beyotime Biotechnology, China) according to the manufacturer's instructions. Protein concentration was determined using the Pierce BCA Protein Assay Kit (Thermo Fisher Scientific, USA). Protein separation and detection were conducted with the automated Jess capillary-based electrophoresis system using the manufacturer's protocol (Protein Simple), using the following antibodies: anti-human GNLY (clone RB1) and anti-human GNLY (clone DH2). Total protein concentration was acquired by total protein detection module (Protein Simple, USA) and was used as a loading control. Chemiluminescence signals were analyzed using Compass for SW software (Protein Simple, USA).

Cytokine measurements

An Aimplex multiplex immunoassays technology – based kit (Quantobio, Beijing, China) was used for the detection of plasma MIG, IP-10, MCP-1, IL-6, IL-7, IL-12p70, IL-15 and IL-18 according to the manufacturer's instructions. The beads, pre-designed according to detection requirements, bind to an antibody specific to a particular cytokine, capturing a target protein molecule from the sample. The detailed experimental process involved the slow thawing of frozen plasma samples, a 60-minute incubation to allow antigen capture by antibody-conjugated bead, a 30-minute incubation of biotinylated-antibody detection of targets, and a 20-minute streptavidin-PE incubation step. Concentrations of cytokines in the samples were determined by comparing the fluorescent signals of samples against a standard curve generated from serial dilutions of known concentrations of the standards. The fluorescence intensities of the beads were measured using a FACS Canto II flow cytometer (BD Biosciences). Each sample was tested in duplicate and the mean of the duplicates was used for analysis. The data were processed using FCAP Array 3.0 software.

Plasma concentrations of soluble CD14 (sCD14) and peptidoglycan recognition proteins (PGRPs) were detected using enzyme-linked immunosorbent assay (ELISA). Human CD14 (R&D Systems, USA) and human PGRPs (FineTest, China) were used, following the manufacturer's instructions. Plasma samples were diluted 1:500 for sCD14 and 1:2 for PGRPs before detection.

The concentration of monokine induced by interferon-gamma (MIG) and interferon gamma-inducible protein 10 (IP-10) in the cell culture supernatant was also detected by ELISA. Human CXCL9/MIG ELISA kit (Multi Sciences, China) and human CXCL10/IP-10 ELISA kit (Multi Sciences, China) were used, following the manufacturer's instructions. The cell culture supernatant samples were diluted 1:100 for MIG and IP-10 before dection.

In vitro cytokine and TCR stimulation experiment

After thawing, magnetically sorted CD8+ T cells were seeded into 96-well plates at a density of 3×10^5 cells per well and stimulated for 48 hours with IL-12 (50 ng/mL, Biolegend), IL-15 (50 ng/mL, Biolegend), IL-18 (50 ng/mL, Biolegend), and CD3/CD28 (25 μg/mL, STEMCELL, Canada). Subsequently, the cells were stained for flow cytometry analysis as described previously.

Cell culture and co-culture

The THP-1 and NCM460 cell lines were cultured in growth medium composed of RPMI 1640 (Gibco, USA), supplemented with 10% fetal bovine serum (Gibco, USA), and 100 U/mL penicillin–streptomycin (Invitrogen, USA), under standard conditions of 5% CO_2 at 37°C. Cells from the third to fifth passages were used for all experiments.

CD8+ T cells were isolated from PBMCs using CD8-positive magnetic bead sorting (Miltenyi Biotech, Germany) and subsequently stimulated with IL-15 (50 ng/mL) for 48 hours. Phorbol 12-myristate 13-acetate (PMA) (20 ng/ml, Merck, Germany) was added during the last 2 hours of stimulation, and the undiluted supernatant was harvested for subsequent use.

In the monocyte stimulation experiment, THP-1 cells, which had been serum-starved overnight, were treated with one of the following: fresh culture medium, the collected supernatant, supernatant containing CD8+ T cells, or supernatant pre-incubated with anti-GNLY antibodies (BioLegend, clone DH10) at 37°C for 30 minutes. After 48 hours of co-culture, the supernatant from THP-1 cells was collected for ELISA analysis.

For the intestinal epithelial cell stimulation experiment, NCM460 cells were pre-seeded into a 24-well plate at a density of 1×10^5 cells per well. After adherence, the medium was replaced with fresh medium, the collected supernatant, or supernatant pre-incubated with anti-GNLY antibodies (BioLegend, clone DH10) at 37°C for 30 minutes. Following 48 hours of culture, the cells were harvested using trypsin. The cell suspension was then dropped onto glass slides, fixed with 4% paraformaldehyde for 15 minutes, and subjected to immunofluorescence staining and analysis.

Immunofluorescence

The fixed NCM460 cells were incubated with the following primary antibodies at 37°C for 60 min: anti-Claudin (1:1500 dilution, Abcam, UK), anti-ZO-1 (1:1800 dilution, Abcam, UK), and anti-Haptoglobin

(1:2000 dilution, Proteintech, China). Subsequently, HRP-conjugated goat anti-mouse/rabbit IgG secondary antibodies were applied and incubated at 37°C for 10 minutes. Signal amplification was then performed using a 1× tyramine signal amplification solution, and cell nuclei were counterstained with DAPI. All slides were scanned and imaged using the Vectra 3 Multispectral Imaging System (Akoya Biosciences) at magnifications ranging from 5- 20×. The acquired data were analyzed using ImageScope software (Version 12.4.3.5008). Ten representative fields per image were selected, and semi-quantitative analysis of mean fluorescence intensity was performed using ImageJ software.

Statistical analysis

Data were statistically performed using IBM SPSS Statistics version 27, while data visualization was conducted through GraphPad Prism software (version 8.3.0) and Origin (version 2022). The Mann–Whitney U test was used to compare the difference between two unpaired groups, and Kruskal–Wallis test was used to compare the multiple groups. Results are shown as medians with quartiles (Q25, Q75). Values were considered statistically significant at a two-tailed and $p < 0.05$.

Results

Perturbations of TCRβ repertoire in PLWH

To explore the impact of HIV infection on TCR repertoire, we conducted a cross-sectional study analyzing TCRβ gene profiles from bulk RNA sequencing data in 228 PLWH and 257 age – and gender-matched healthy controls (HC) (Figure 1(A), Supplementary Table 1). Compared to HC, the usage of V/Jβ genes in PLWH was notably disrupted. Among functional human Vβ/Jβ genes, 34 Vβ and 3 Jβ genes showed significant differences between the two groups (Supplementary Figure 1A, B). Additionally, the length of the third complementary-determining region (CDR3) similarly exhibited Gaussian-like distribution, peaking at 13-amino acids. However, the proportions of 7-, 8-, 9-, 10-, 11 – and 16-amino acids differed significantly between these two groups (Supplementary Figure 1C). Visualizations of TCR Vβ – Jβ gene usage combinations revealed that nearly 70% of HC exhibited uniform gene combinations (Supplementary Figure 1D 1-5), and the remaining 30% displayed biased gene usage (Supplementary Figure 1D 6-8). In contrast, over 50% of PLWH displayed a notably high proportion of specific gene usage (Supplementary Figure 1E 1-8). Significant perturbation in TCR V/Jβ gene usage indicates that HIV-1 infection modifies the clonality and diversity of TCRβ repertoire.

To further quantify the impact of HIV infection on TCR repertoire, we compared the clonality and diversity between HC and PLWH groups. The results revealed that PLWH had significantly elevated numbers of large and big clones compared to HC. Specifically, the median values for large clones were 7 in PLWH versus 4 in HC, and for big clones, 46 in PLWH versus 33 in HC (Figure 1(B,C)). We also calculated the percentage of the top 10 and top 20 most abundant clones in the TCRβ repertoire, which confirmed that PLWH exhibited higher levels of clonal expansion. The top 10 and top 20 clones accounted for 18.5% and 22.8% of the total T cell repertoire in PLWH, compared to 14.3% and 17.2% in HC (Figure 1(D,E)). In terms of diversity, the Richness, Shannon entropy, and D50 indices were significantly reduced in PLWH compared to HC, while the Gini coefficient was markedly higher (Supplementary Figure 2A). These findings indicate a significant clonal expansion in the TCRβ repertoire of PLWH, along with a substantial reduction in diversity.

Given the significant heterogeneity among PLWH, we first categorized them into treatment-naïve patients (TP) and those receiving ART. The ART group was further subdivided based on treatment duration: less than 24 months (<24 m) and more than 24 months (>24 m) (Supplementary Table 1). We found that as the ART duration increased, clonality and diversity gradually approached HC levels (Figure 1(F–I), Supplementary Figure 2B), and these four clonal metrics negatively correlated with ART duration time (Supplementary Figure 3A). However, it is worth noting that, compared to the TP group, there was no significant recovery in clonality and diversity in the <24 m group. Even beyond 24 months, ART still did not fully restore the normal TCRβ repertoire, with higher clonality and lower diversity compared to HC. These data suggest that prolonged ART therapy can partially but not completely restore the clonal expansion in the TCRβ repertoire.

Most PLWH achieved virological suppression within 1–3 months after ART, while only a minority of patients continued to have detectable viral loads or experienced virological rebound after three months. Consequently, we divided the <24 m group into two subgroups based on their virological response to ART: “fast responders,” who achieved undetectable viral loads within 3 months, and “slow responders,” who took longer than 3 months to reach undetectable levels. We observed that individuals with a rapid treatment response exhibited lower clonality and higher diversity (Figure 1(J–M), Supplementary Figure 2C), indicating that the extent of clonal expansion is correlated with treatment efficacy. Individuals with ART over 24 months were further categorized into immunological responders (IR) and immunological non-responders (INR) groups based on their CD4+

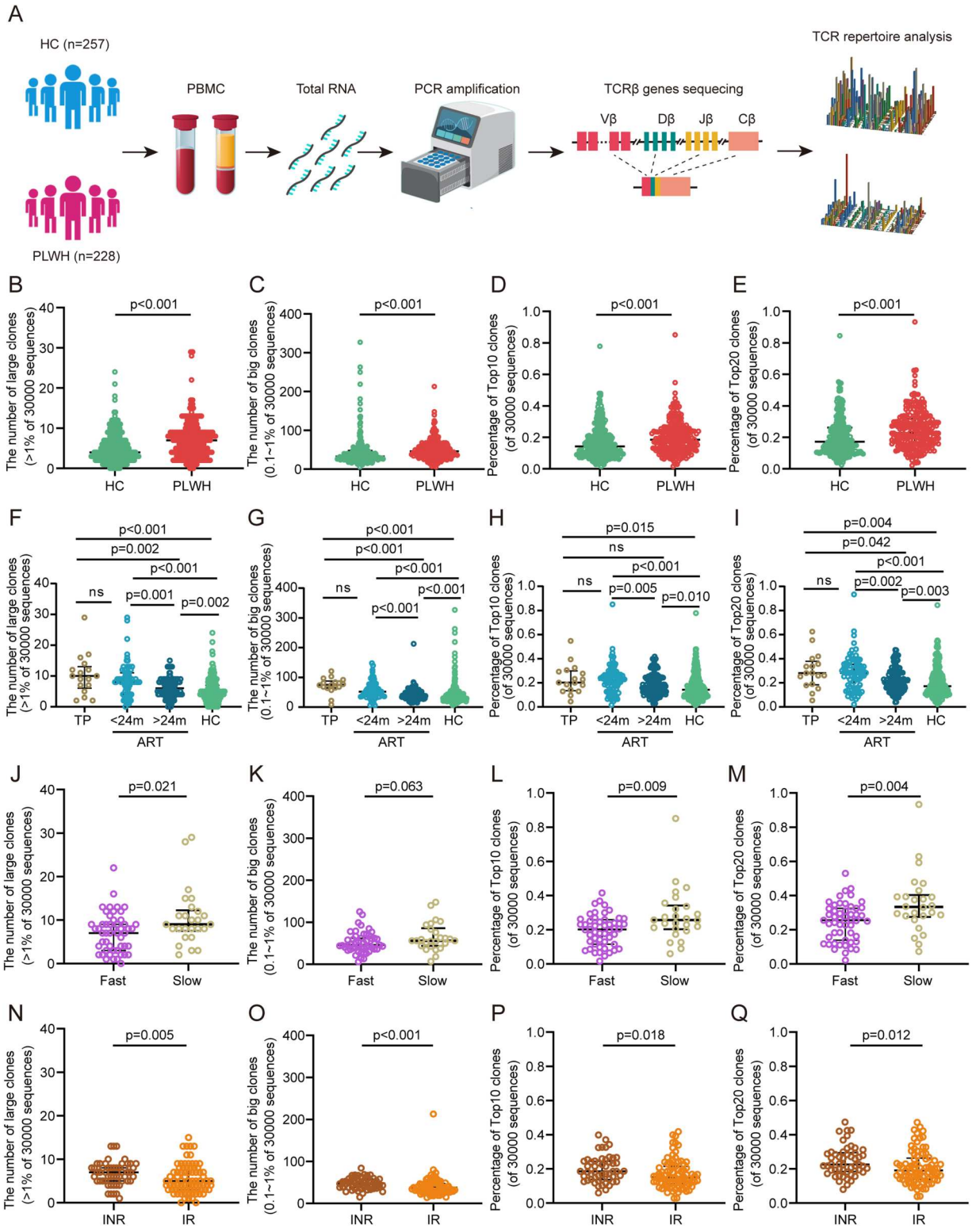

Figure 1. Perturbations of TCRβ clonality in PLWH. (A) Schematic diagram of the workflow for bulk TCR*β* sequencing. (B-Q) Scatter plots showing TCRβ clonality metrics, normalized to 30,000 total sequences, across different groups. (B, F, J, N) Number of large clones; (C, G, K, O) number of big clones; (D, H, L, P) percentage of top 10 clones; (E, I, M, Q) percentage of top 20 clones. Comparisons are shown between: (B-E) healthy controls (HC, $n = 257$) and people living with HIV (PLWH, $n = 228$); (F-I) treatment-naive patients (TP, $n = 17$), ART less than 24 months (<24 m, $n = 77$), ART more than 24 months (>24 m, $n = 134$), and HC; (J-M) fast and slow virological response groups; (N-Q) immune non-responders (INR, $n = 53$) and immune responders (IR, $n = 81$).

T cell counts. The clonality and diversity in IR were better restored than INR (Figure 1N-Q, Supplementary Figure 2D). Moreover, clonal expansion indices were significantly negatively correlated with CD4 counts and CD4/8 ratio, and positively correlated with CD8 counts for IR and INR (Supplementary Figure 3B-D). These findings indicate that T cell clonal expansion is an indicator of treatment duration, therapeutic response and immune recovery in the context of PLWH.

Features of TCRβ repertoire extrapolate accelerated aging in PLWH

Recent studies have shown that a TCR clock exists in healthy individuals; that is, the TCR repertoire exhibits an age-related trend and can serve as a predictor of biological age [19,26,27]. However, it remains unclear whether HIV infection disrupts this clock. Building on this premise, we initially stratified HC and PLWH into three groups according to WHO guidelines: young (18–44 years old), middle-aged (45–59 years old), and elderly (≥60 years old). We found that compared with HC, clonality was significantly accelerated and diversity decreased in both young and middle-aged PLWH groups, but there was no significant difference in the elderly group (Figure 2(A–D), Supplementary Figure 4A-D). These results suggest that HIV infection contributes to increased T-cell clonal expansion, particularly in younger populations. Interestingly, no discernible differences were observed between the young and middle-aged groups within HC (except for the Richness). In contrast, the elderly group exhibited increased clonality and reduced diversity compared to the middle-aged group. Conversely, in PLWH, significant differences were found between the young and middle-aged groups (except for the number of big clones). At the same time, clonal expansion and diversity levels remained consistent between the elderly and middle-aged groups. These findings suggest that PLWH may experience premature aging.

vRecent studies indicate that human aging is not linear, with potential cliff-like aging nodes at specific points [28,29]. To further explore the aging changes in PLWH, we conducted a polynomial regression analysis on eight indicators with age. The results were consistent across the indicators, with D50 showing the most pronounced trend (Figure 2(E–H), Supplementary Figure 4E-H). HC displayed a nonlinear aging profile, with accelerated changes occurring before the age of 30 and after 55, while the period

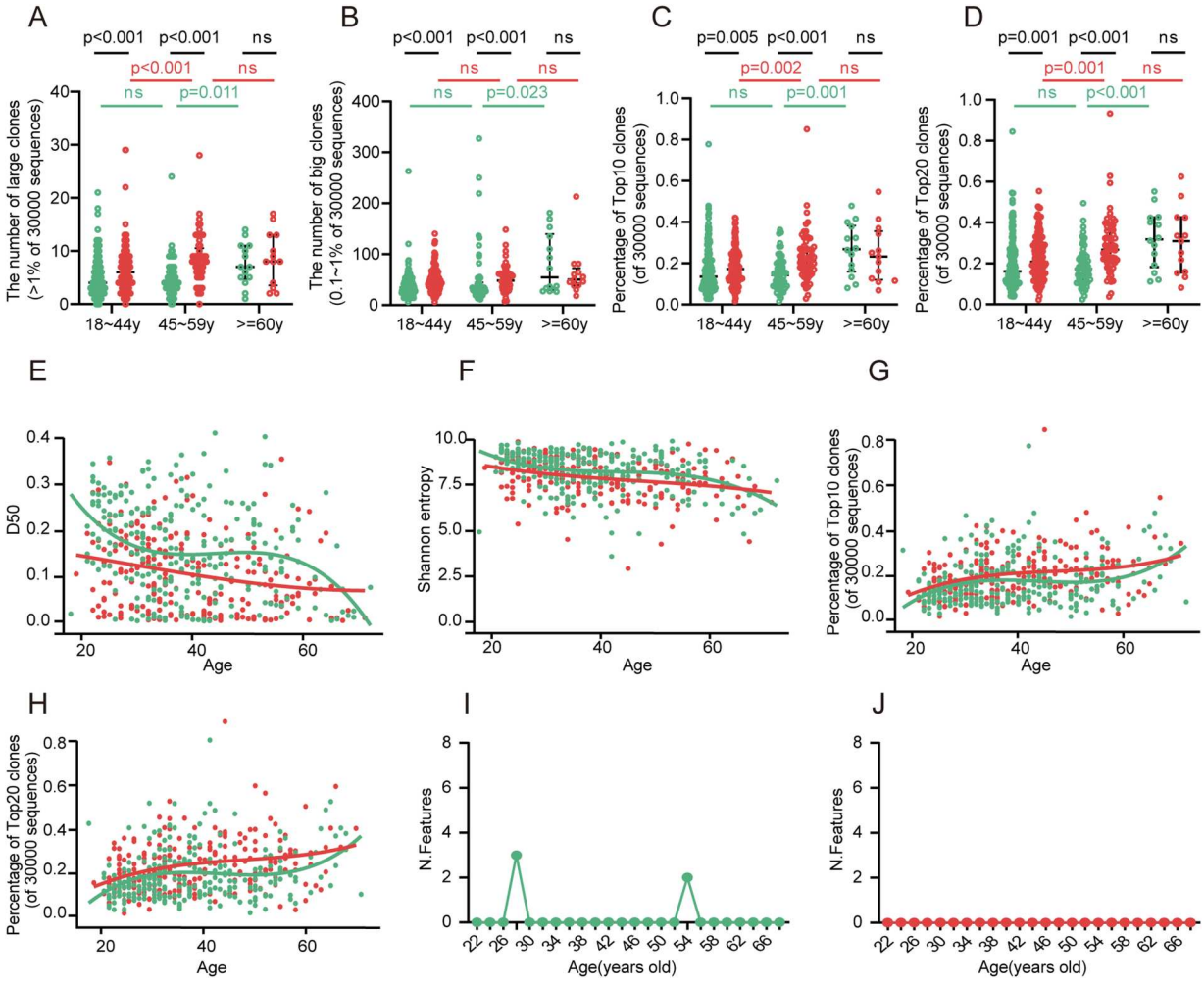

Figure 2. Age-associated changes of TCR repertoire in HC and PLWH. (A-D) Scatter plots showing age-associated changes in clonality metrics for HC (blue dots) and PLWH (red plots). Each dot corresponds to an individual sample. Statistical comparisons are indicated by lines: black lines for comparisons between HC and PLWH, green lines for within-HC comparisons, and red lines for within-PLWH comparisons. (E-H) Polynomial regression analysis of TCR repertoire metrics with age: (E) D50, (F) Shannon entropy, (G) percentage of top 10 clones and (H) percentage of top 20 clones. Regression lines are shown for HC (green) and PLWH (red). (I-J) Sliding window analysis of age-associated changes in differentially presented features for (I) HC and (J) PLWH.

between 30 and 55 years old represents a relative plateau. However, PLWH showed a more linear pattern of accelerated aging after infection. Notably, the aging level of PLWH at 20 years old already matches or even exceeds the plateau level observed in HC aged 30–55, with a crossover point occurring around 65 years old. Additionally, using sliding window analysis, we found that HC displayed two distinct aging peaks, around 28 and 54 years old (Figure 2(I)), with significant differences in Shannon entropy and percentage of top10/top20 clones. In contrast, PLWH did not show any such peaks, which aligns with the polynomial regression analysis (Figure 2(J)). These findings suggest that HIV infection disrupts the phased aging model seen in HC, resulting in continuous aging acceleration, with young PLWH exhibiting significantly higher levels of aging compared to HC.

GNLY+CD8+ T cells were the primary cell population for clonal maintenance and expansion

To overcome the limitations of bulk TCR sequencing in distinguishing T cell subgroups and allow deeper exploration of clonally expanded cell phenotypes, we enrolled another cohort of sorted CD4 + and CD8+ T cells with single-cell RNA paired with TCR sequencing data from HC ($n = 4$) and PLWH ($n = 9$), including TP ($n = 6$) and ART ($n = 3$) individuals (paired with TP cases) (Supplementary Figure 5A)[2]. We obtained 51,747 CD4+ T and 53,570 CD8+ T cells, paired with 40,289 and 22,974 unique TCRs, respectively (Supplementary Figure 5B-C). Dimensional reduction analysis (uniform manifold approximation and projection, UMAP) was applied to CD8+ T and CD4+ T cells. By pairing TCR information with phenotypic data, we observed that cells exhibiting high-frequency clonal expansion were predominantly localized within the CD8+ T cell population (Supplementary Figure 5D). Subsequently, clonal cells were categorized as hyperexpanded (>10% of total unique clones), large (1–10%), medium (0.1–1%), small (<0.1%), and unique clones (no clonal expansion). Across HC, TP, and ART groups, CD4+ T cells were primarily composed of unique clones. In contrast, CD8+ T cells in HC contained a small number of medium and small clones, while the proportion of hyperexpanded, large, medium, and small clones increased significantly to nearly 75% in TP, and decreased after ART but remained significantly higher than in HC (Supplementary Figure 5E). These results underscored that CD8+ T cell clonal expansion is greater than that of CD4+ T cells, which aligns not only with observations in other diseases [30,31], but also with the persistence of elevated CD8 + T cell counts in PLWH, even after 12-year ART [12].

To further dissect the features of clonally expanded cells, we performed cluster analysis on positively related genes with a correlation coefficient (r) greater than 0.1. Two distinct gene clusters were identified (Figure 3(A)). UMAP visualization revealed that cluster 2 genes were primarily concentrated in regions with high clonal expansion (marked by a red circle), and cluster 1 genes were evenly distributed across the entire landscape (Figure 3(B)). We further identified overlapping clones within each individual for the three individuals with paired TP and ART samples. The overlapping clones were categorized as expanded, contracted, or stable based on their post-ART frequency (Figure 3(C)). Consistently, cluster 2 genes showed high expression in expanded and stable clones (Figure 3(D)), confirming these genes were intimately associated with clonal expansion and maintenance.

Next, we aimed to identify appropriate phenotypic markers of clonally expanded cells from these genes positively correlated with clonal frequency. The top 10 genes were GNLY, GZMB, FCGR3A, FGFBP2, GZMH, KLRD1, PRF1, NKG7, PRSS23 and CST7, all belonging to cluster 2 genes (Figure 3(E)). These genes exhibited varying degrees of high expression in the clonal expansion regions (Supplementary Figure 6A). Notably, GNLY, FCGR3A and PRSS23 were primarily concentrated in high clonal expansion regions, suggesting these genes may be specific markers for highly clonally expanded cells. In contrast, the other genes were generally expressed across broader regions, suggesting their relatively low specificity for clonal expansion. To identify practical indicators of clonal expansion in vitro, we used flow cytometry to verify the expression of these proteins. Due to the availability of corresponding flow antibodies, we successfully verified the expression of five proteins—GNLY, GZMB, CD16, CD94 and Perforin —corresponding to the genes GNLY, GZMB, FCGR3A, KLRD1 and PRF1, respectively. Among these genes, GNLY emerged as the top candidate, demonstrating distinct clustering at the protein level and being gateable. In contrast, CD16 and CD94 exhibited lower protein levels and were ineffective as indicators of clonal expansion. GZMB showed a positive expression rate exceeding 50%, whereas perforin displayed less distinct clustering characteristics. Co-expression analysis further revealed that approximately 98.37% of GNLY+CD8+ T cells co-expressed GZMB, and 62.26% co-expressed perforin, indicating strong consistency between GNLY and these genes (Supplementary Figure 6B). Collectively, these findings suggest that GNLY serves as the optimal marker for identifying CD8+ T cells with high clonal expansion.

Furthermore, sc-RNA sequencing data analysis revealed that the proportion of clonally expanded cells among GNLY+CD8+ T cells reached up to 80% across HC, TP, and ART groups. The proportions of

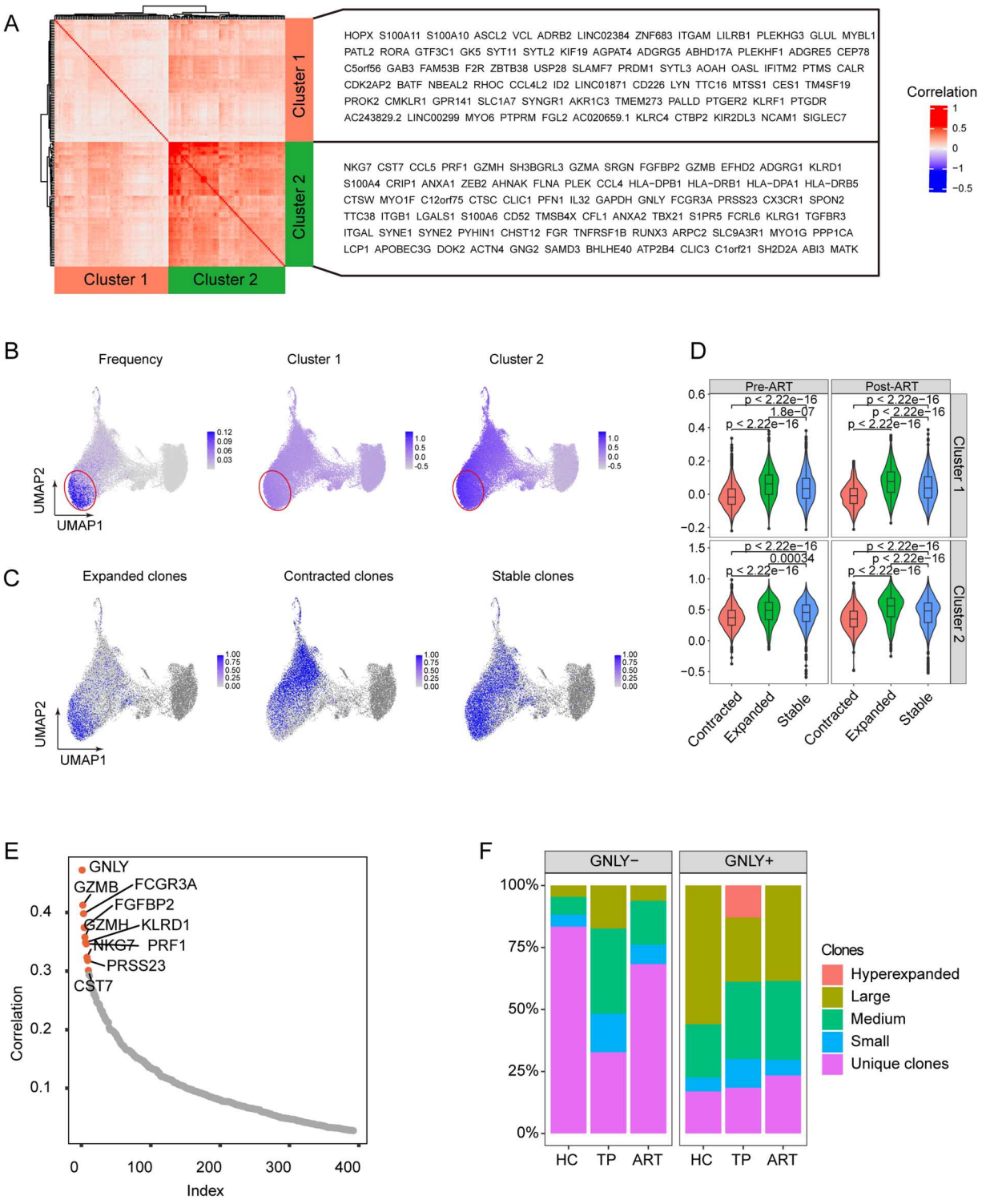

Figure 3. GNLY as an optimal marker for highly clonally expanded CD8+ T cells. (A) Heatmap showing two clusters of genes positively associated with clonal frequency of CD8+ T cells ($p < 0.01$, $r > 0.1$). (B) UMAP plots depicting the clonal frequency and expression distribution of two gene clusters in CD8+ T cells. Red circles highlight regions of high clonal expansion. (C) UMAP plots visualizing expanded, contracted, and stable clones from overlapping clonal populations in three paired patients, with color gradients representing cell density. (D) Violin plots comparing the expression scores of two gene clusters in expanded, contracted, and stable clones pre – and post-ART. (E) Scatter plots illustrating genes positively correlated with the clonal frequency of CD8+ T cells. The top 10 correlated genes are highlighted in red. (F) Bar plots showing the clonal size distribution of GNLY-CD8+ T cells and GNLY+CD8+ T cells across HC, TP, and ART groups. Clones are categorized as hyperexpanded (>10% of total unique clones), large (1–10%), medium (0.1–1%), small (<0.1%), and unique (no clonal expansion).

hyperexpanded and large clones were significantly higher in GNLY+CD8+ T cells compared to GNLY-CD8+ T cells, indicating that GNLY+CD8+ T cells serve as a highly specific marker for clonally expanded cells. In contrast, GNLY-CD8+ T cells only exhibited an increased proportion of clonally expanded cells during TP, which significantly decreased after ART (Figure 6(F)). Validation using three matched samples

pre – and post-ART confirmed this trend (Supplementary Figure 6C, D), demonstrating that GNLY +CD8+ T cells not only represent a highly clonally expanded cell population but also exhibit robust clonal maintenance potential.

GNLY+CD8+ T cells exhibit enhanced cytotoxicity and low exhaustion characteristics

To reveal the phenotypic characteristics of persistent clonal cell populations, we analyzed them at both the transcriptional and protein levels. The genes in cluster 2 were primarily enriched in cell killing, positive regulation of cell activation, and NK cell-mediated cytotoxicity processes, while genes in cluster 1 were enriched in cell differentiation, migration and activation pathways (Figure 4(A)). Subsequently, we included 10 HC and 64 PLWH (18 TP, 23 IR and 23 INR) (Supplementary Table 2) for flow cytometry validation. The proportion of GNLY+CD8+ T cells was significantly elevated in PLWH and increased further after ART, with the INR group showing a notably higher proportion than the IR group (Figure 4(B)). The number of these cells increased significantly in PLWH, and there was no significant difference across the TP, IR and INR groups (Supplementary Figure 7A). This finding aligns with the characteristics of clonal maintenance and expansion observed in the transcriptional level, where the proportion increases post-ART relative to the contraction of other clonal populations, while the absolute count remains stable.

Additionally, CCR7 and CD45RA expression analysis revealed that this cell population was mainly of the terminally differentiated phenotype (Temra, CD45RA + CCR7−) (Supplementary Figure 7B). Correlation analysis showed that the proportion of GNLY +CD8+ T cells in post-ART samples was positively correlated with age ($r = 0.402$, $p = 0.013$) and negatively correlated with the CD4/CD8 ratio ($r = -0.496$, $p = 0.002$). Additionally, the absolute count of GNLY+CD8+ T cells also showed a tendency of positive correlation with age ($r = 0.306$, $p = 0.065$) and a negative correlation with the CD4/CD8 ratio ($r = -0.457$, $p = 0.004$) (Supplementary Figure 7C, D). These results suggest that GNLY+CD8+ T cells are closely associated with aging and clinical indicators that reflect disease prognosis.

To further analyze the phenotypic changes of these cells across different groups, GNLY-CD8+ T and GNLY+CD8+ T cells were gated in HC, TP, IR and INR groups, respectively. We found that GNLY +CD8+ T cells exhibited lower activation levels of HLA-DR and CD38 compared to GNLY-CD8+ T cells. However, these activation indexes were significantly higher in PLWH than in HC, with the highest levels observed in the TP group and INR levels surpassing IR after ART (Figure 4(C), Supplementary Figure 7E). Moreover, GNLY+CD8+ T cells showed a significant decrease in co-stimulatory molecules of CD27 and CD28 in contrast to GNLY-CD8+ T cells, with PLWH displaying lower levels than HC (Figure 4(D), Supplementary Figure 7F). Alongside this, there was an increase in the aging marker CD57, with PLWH showing higher CD57 levels than HC, which continued to rise after ART (Figure 4(E), Supplementary Figure 7G), indicating pronounced aging characteristics in this cell population. Despite these aging characteristics, GNLY+CD8+ T cells demonstrated downregulation of PD-1 (Figure 4(F), Supplementary Figure 7H), indicating reduced exhaustion, along with an enhanced cytotoxic phenotype characterized by elevated levels of GZMB, Perforin, CX3CR1 and T-bet (Figure 4(G), Supplementary Figure 7I). Additionally, there was upregulated expression of NK cell receptors such as KLRG1 and NKG2D (Figure 4(H), Supplementary Figure 7J). These changes were more pronounced in PLWH than in HC. These findings suggest that GNLY+CD8+ T cells are characterized by enhanced cytotoxicity and low exhaustion.

Bystander expansion of GNLY+CD8+ T cells

To explore potential driving signals for CD8+ T-cell clonal expansion, we divided CD8+ T cells into five subsets (C01 – C05) based on the expression profiles of canonical gene markers (Figure 5(A,B)). As expected, the C03 subset exhibited significantly high expression of the GNLY gene, was predominantly enriched in regions of high clonal expansion, and its proportion continued to increase after ART (Figure 5(C)). We further evaluated TCR-dependent signaling pathways and bystander activation pathways in the C03 subset [32]. The results revealed that most TCR-dependent signaling pathways and bystander activation pathways in the C03 subset were significantly enhanced during TP. However, after ART, most TCR signaling pathways showed a downregulation trend, whereas bystander activation pathways were maintained or further enhanced (Figure 5(D)). These findings suggest that enhanced bystander activation pathways may be a key driver of the sustained clonal expansion of GNLY +CD8+ T cells in PLWH after ART.

To verify the role of the bystander activation pathway, we evaluated cytokine receptor expression on GNLY+CD8+ T cells. We found that, compared to HC, the expression levels of CD122, CD212 and CD218 were significantly upregulated in PLWH. Moreover, CD127, CD122 and CD218 levels continued to increase after ART, with INR levels surpassing those of IR (Figure 5(E), Supplementary Figure 7K). We further measured the plasma levels of the cytokines corresponding to these receptors and found that only IL-18 levels were significantly higher in

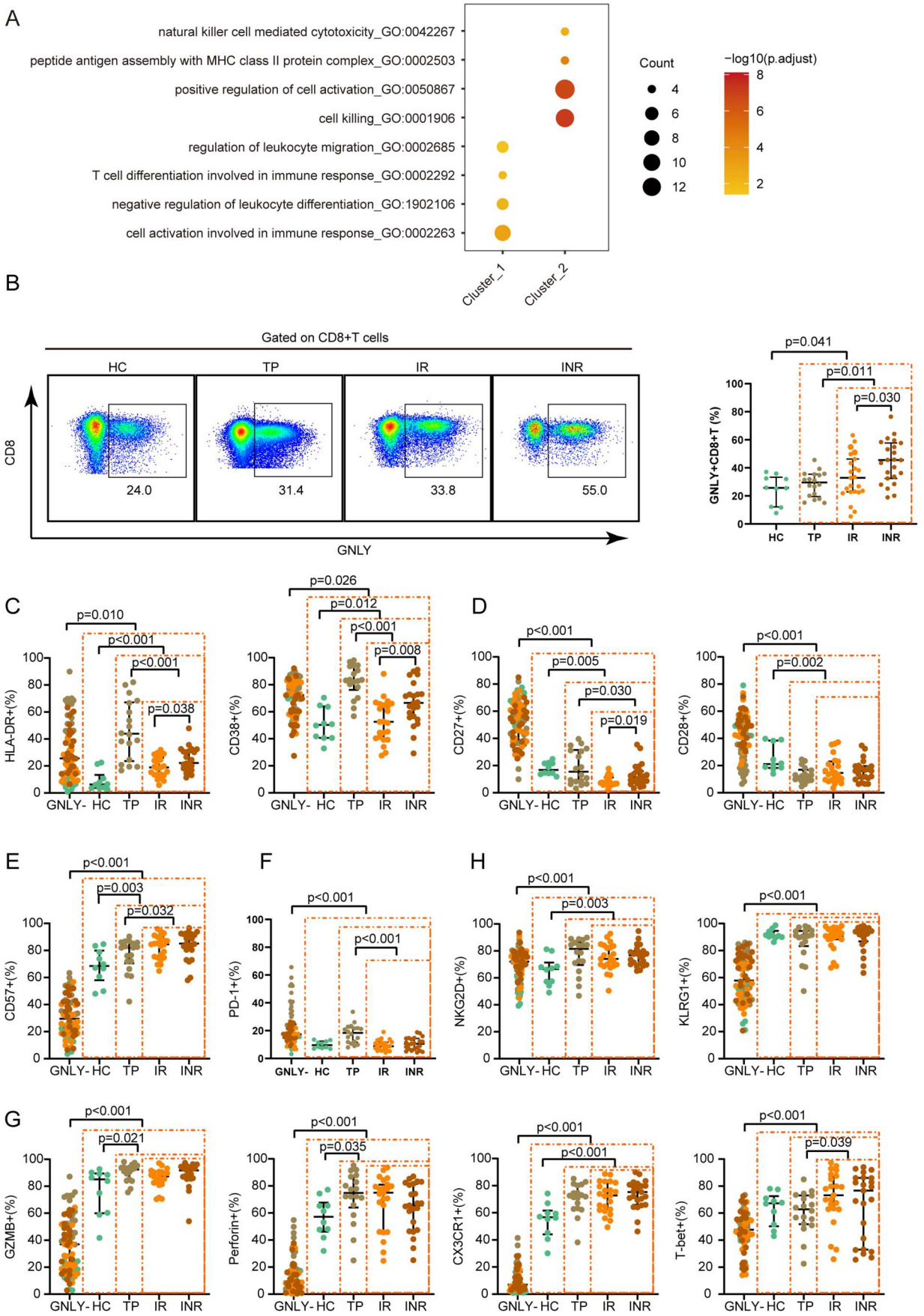

Figure 4. Enhanced cytotoxicity and low exhaustion in GNLY+CD8+ T cells. (A) Gene enrichment analysis of two clusters of genes associated with clonal frequency ($p < 0.01$, $r > 0.1$) (B) Representative flow cytometry and scatter plots comparing GNLY-CD8+ T with GNLY+CD8+ T cells, as well as differences among GNLY+CD8+ T cells across groups. (C-H) Comparison of marker expression between GNLY-CD8+ T cells and GNLY+CD8+ T cells, as well as among GNLY+CD8+ T cell groups. (C) HLA-DR and CD38; (D) CD27 and CD28; (E) CD57; (F) PD-1; (G) GZMB, Perforin, CX3CR1, and T-bet; (H) NKG2D and KLRG1. The dashed box indicates samples that are analyzed collectively as a unified group. The GNLY+CD8+ T cell groups include HC ($n = 10$), TP ($n = 18$), INR ($n = 23$) and IR ($n = 23$); the PLWH group comprises TP, IR and INR; and the ART group includes IR and INR.

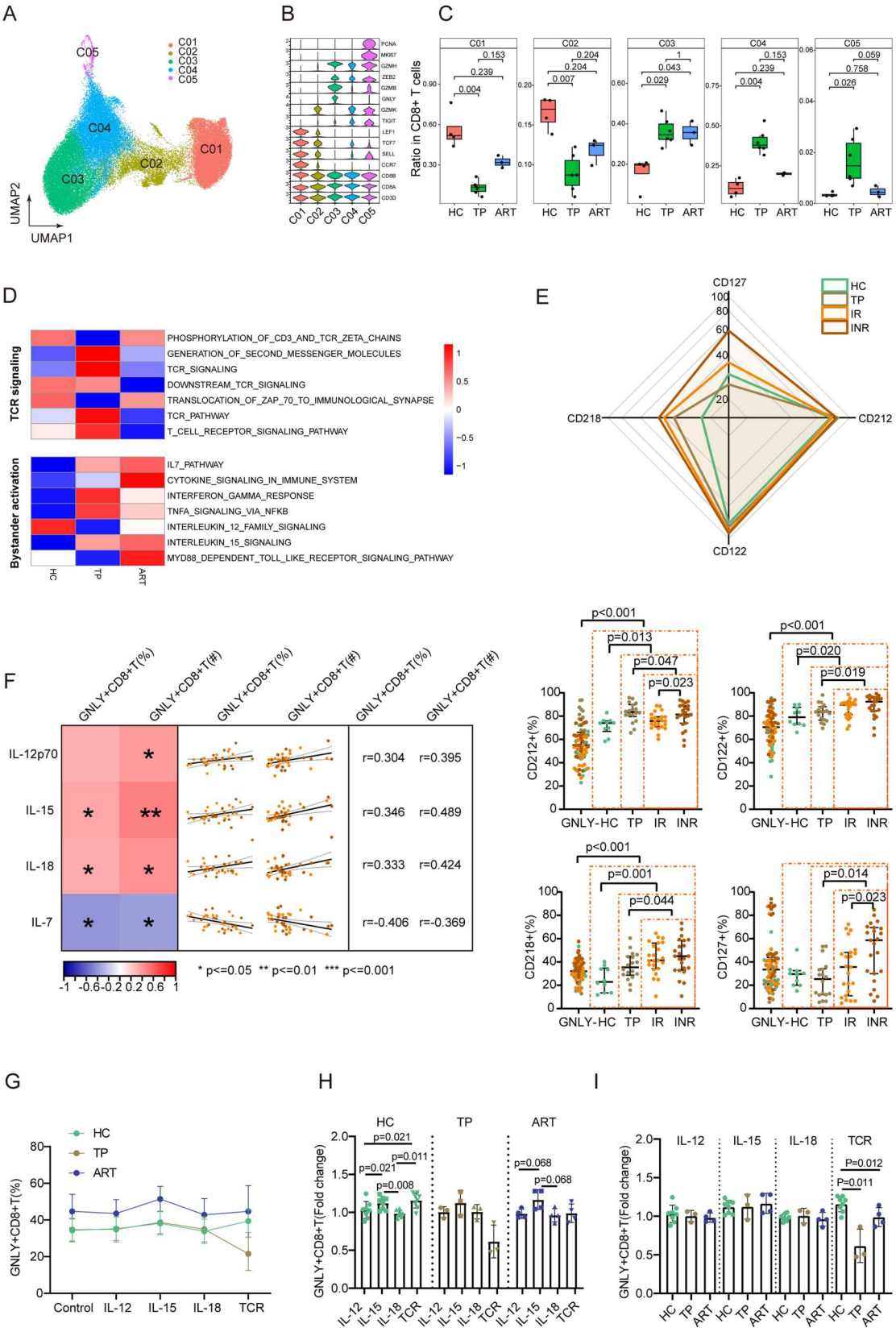

Figure 5. Enhanced bystander activation pathway in GNLY+CD8+ T cells. (A) UMAP visualization of CD8+ T cell subsets. (B) Violin plots depicting the expression distribution of canonical cell markers across five CD8+ T cell clusters. (C) Box plots showing the proportions of five CD8+ T cell subsets in HC, TP and ART groups. Each point represents one sample. (D) Heatmap displaying gene set activities of C03 subset, quantified as normalized enrichment scores (NES) from GSEA, for TCR-dependent and bystander activation pathways. (E) Radar chart and scatter plots showing the relative expression levels of CD127 (IL-7R), CD212 (IL-12R), CD122 (IL-15R) and CD218 (IL-18R) across HC ($n = 10$), TP ($n = 18$), IR ($n = 23$) and INR ($n = 23$) groups. (F) Heatmap, correlation plots and r-value demonstrating the correlation among the proportion and absolute count of GNLY+CD8+ T, as well as the plasma level of IL-7, IL-12p70, IL-15 and IL-18 in both IR and INR groups. (G-I) Line plots and scatter plots depicting changes in(G) the proportion and (H, I) fold change of GNLY+CD8+ T cells in HC, TP, and ART after different stimulation. Fold change values (H, I) are calculated relative to the control group. Control, medium; TCR, CD3/28 T cell activator.

PLWH compared to HC, with an increasing trend after ART (Supplementary Figure 8A-D). Correlation analysis revealed a significant positive correlation between the proportion of GNLY+CD8+ T cells and both plasma levels of IL-15 and IL-18. Additionally, the absolute count of GNLY+CD8+ T cells was positively correlated with IL-15, IL-12p70 and IL-18 levels (Figure 5(F)). For further validation, we stimulated CD8+ T cells in vitro using IL-12, IL-15, IL-18, and CD3/CD28 antibodies to mimic bystander activation pathways and TCR-dependent signaling pathways, respectively. The results revealed that IL-15 significantly increased the proportion of GNLY+CD8+ T cells in HC, TP, and ART groups, also inducing upregulation of HLA-DR, granzyme B (GZMB), and perforin expression, whereas in the HC group, TCR stimulation produced similar effects, this response level decreased in TP but was partially restored after ART (Figure 5(G–I), Supplementary Figure 9A-C). Collectively, these findings validate that bystander activation pathways play a crucial role in the clonal expansion of GNLY+CD8+ T cells at different stages.

Pro-inflammatory characteristics of GNLY+CD8 + T Cells

GNLY was reported to be expressed late after T cell activation [33], along with the expression of cytotoxic particles including GZMB and perforin. Recent studies have shown that the two isoforms of GNLY have completely different localizations and functions [34–36]. The 9 kDa GNLY, commonly regarded as a cytotoxic effector molecule, is enriched in dense granules along with GZMB and Perforin and capable of directly killing bacteria and other pathogens. In contrast, the 15 kDa GNLY, initially thought to be merely a precursor molecule, has been shown to function as an immune alarmin but lacks cytotoxic activity.

To examine the exact form of GNLY in CD8 + T cells, we first selected two monoclonal antibodies of GNLY for flow cytometry staining, which have been reported that clone RB1 recognizes total GNLY protein, while clone DH2 only recognizes the 9 kDa isoform [37]. We gated the cells with substantial GNLY expression, including NK cells and CD8+ T cells, and compared the proportions of different isoforms of GNLY. As expected, total GNLY (clone RB1) expression on NK cells was significantly higher than that on CD8+ T cells. Notably, the proportions of 9 kDa GNLY (clone DH2) on NK and CD8+ T cells were 38.9% and 4.8%, respectively, and the ratio of 9 kDa/total GNLY was also significantly different between the two cell types (Figure 6(A)). Notably, CD8+ T cells predominantly express 15 kDa GNLY, with a proportion as high as 80%.

To further validate this finding, we initially used magnetic beads to sort NK cells and CD8+ T cells from PBMCs and subsequently used a polyclonal anti-GNLY antibodies (R&D Systems)[38] to distinguish different isoforms of GNLY via digital Western blotting. As shown in Figure 6(B), NK cells exhibited 9 and 15 kDa forms of GNLY, whereas CD8+ T cells only displayed the 15 kDa form. After normalizing for total protein content, it was evident that 9 kDa GNLY was predominantly expressed in NK cells. Conversely, in CD8+ T cells, GNLY was mainly present as the 15 kDa form.

Given the potential pro-inflammatory effects of 15 kDa GNLY, we investigated the levels of inflammatory factors (MIG, IP-10, MCP-1 and IL-6) in the plasma. The results showed that only IP-10 and MIG were significantly higher in PLWH compared to HC, peaking in the TP group and decreasing significantly after ART, with INR levels remaining higher than IR. MCP-1 and IL-6 levels did not show significant statistical differences (Supplementary Figure 8E-J). Since intestinal inflammation is a significant contributor to inflammaging [39], we also examined relevant indicators of intestinal damage and microbial translocation, including Zonulin, PGRPS and sCD14, all of which exhibited significant elevation in PLWH (Figure 6(C,D)). Correlation analysis revealed that the proportion of GNLY+CD8+ T cells was positively correlated with IP-10, MIG, Zonulin, PGRPS and sCD14, and the absolute count was positively correlated with IP-10, MIG, Zonulin and PGRPS (Figure 6(E)), suggesting that GNLY+CD8+ T cells are closely associated with ongoing inflammaging in PLWH.

GNLY derived from CD8+ T cells activates monocytes and disrupt intestinal epithelial cells

To further explore the pro-inflammatory mechanisms of GNLY+CD8+ T cells, purified CD8+ T cells were initially stimulated with IL-15 to upregulate GNLY, and then PMA was added to enhance the release of 15 kDa GNLY into the cell supernatant [38]. Subsequently, the GNLY-enriched supernatant was collected, and fresh culture medium was used as a control for subsequent functional experiments (Figure 7(A)). The results revealed that the supernatant from stimulated CD8+ T cells significantly induced THP-1 cells to secrete IP-10 and MIG, while the combination of stimulated CD8+ T cells and their supernatant exhibited even stronger pro-inflammatory effects. This effect could be partially neutralized by anti-GNLY antibodies, suggesting that GNLY contributes partially to the pro-inflammatory response (Figure 7(B)).

To assess the impact on the intestinal barrier, we used the intestinal epithelial cell line NCM460. The supernatant from stimulated CD8+ T cells significantly disrupted the tight junction proteins Claudin and ZO-1 and induced the upregulation of zonulin

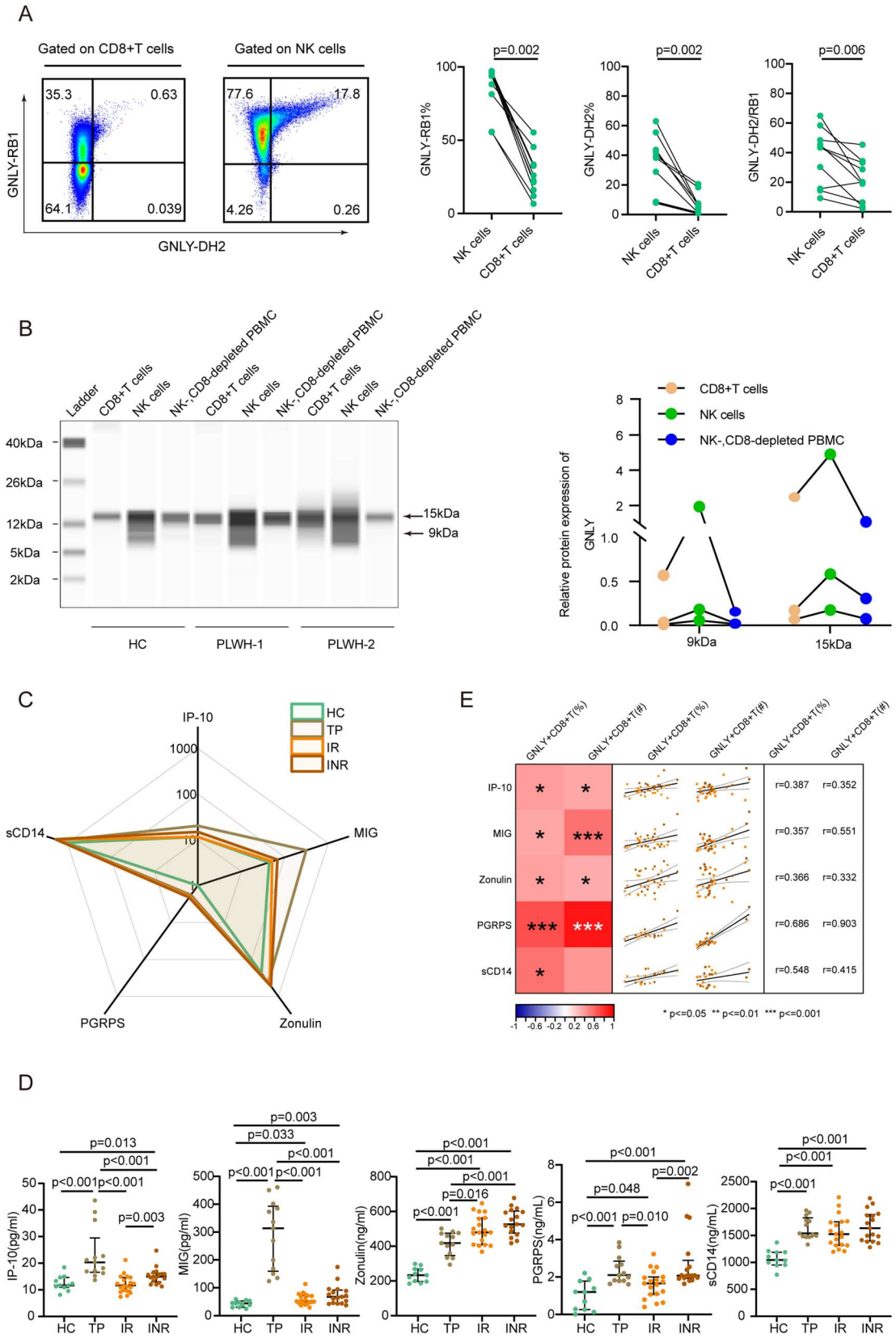

Figure 6. Pro-inflammatory potential of GNLY+CD8+ T Cells. (A) Representative flow cytometry and scatter plots illustrating the distribution of two isoforms of GNLY in NK and CD8+ T cells. (B) Capillary-based automated Western immunoblotting demonstrating protein expression levels of 9 and 15 kDa GNLY protein in isolated NK, CD8+ T and NK-,CD8-depleted PBMC from HC ($n = 1$) and PLWH ($n = 2$). GNLY expression levels were quantified and normalized to the total protein concentration. (C-D) Radar chart (C) and scatter plots (D) depicting the plasma level of IP-10, MIG, zounlin, PGRPS and sCD14 across HC ($n = 11$), TP ($n = 13$), IR ($n = 19$) and INR ($n = 16$) groups. (E) Heatmap, correlation plots and r-value demonstrating the correlation among the proportion and absolute count of GNLY+CD8+ T, as well as the plasma level of IP-10, MIG, Zonulin, PGRPS and sCD14 in both IR and INR groups.

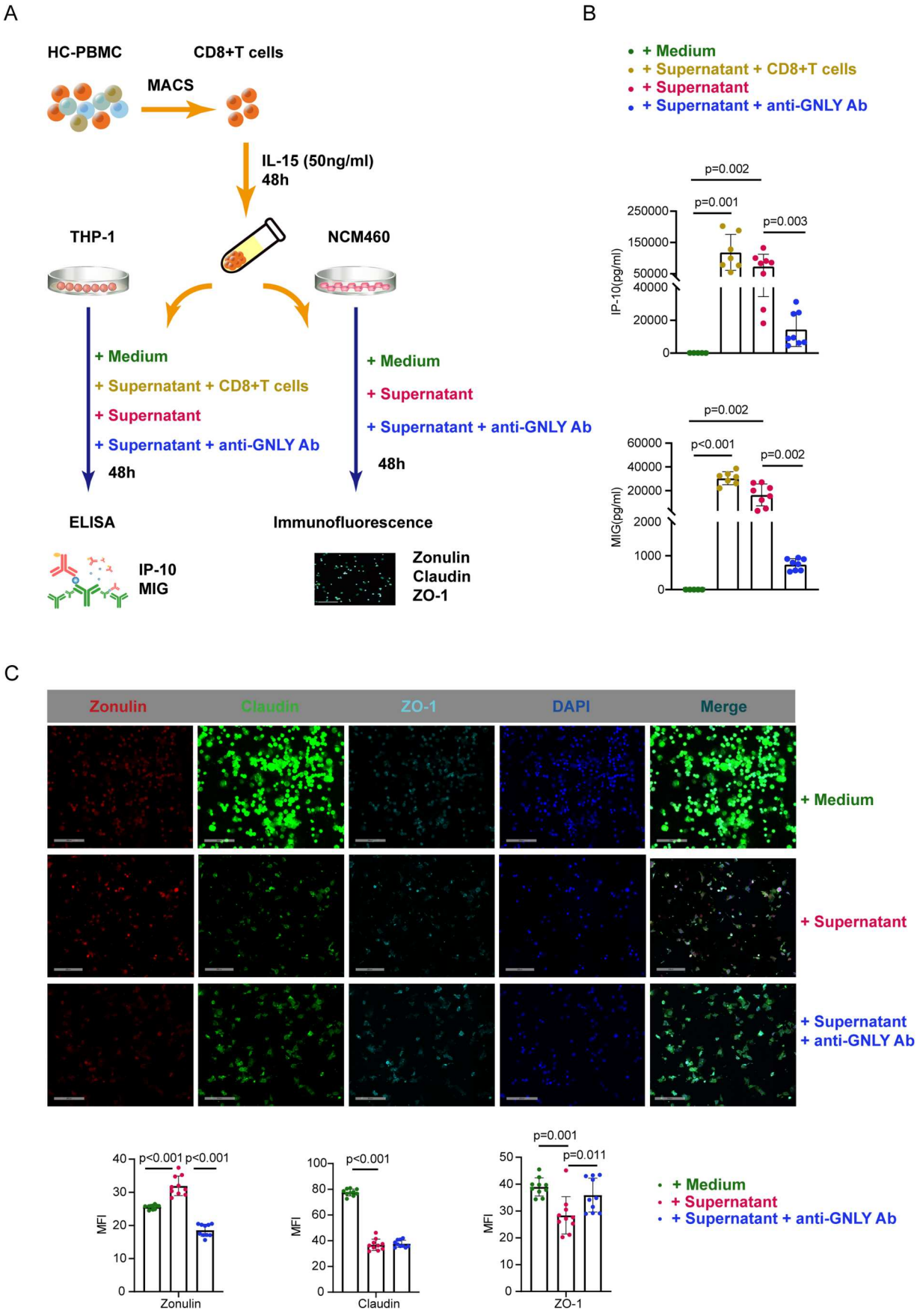

Figure 7. GNLY derived from CD8+ T cells activates monocytes and disrupt intestinal epithelial cells. (A) Schematic diagram depicting the workflow of the functional co-culture experiment. (B) Bar plots displaying the levels of IP-10 and MIG in the supernatant of THP-1 cells after 48 hours of co-culture across experimental groups. (C) Representative immunofluorescence images and statistical plots illustrating the expression levels of Zonulin, Claudin, and ZO-1 in NCM460 cells after 48 hours of co-culture.

(Figure 7(C)). Similarly, anti-GNLY antibodies partially reversed this effect, indicating that GNLY directly disrupts the intestinal barrier. Collectively, these findings demonstrate that GNLY+CD8+ T cells play a significant role in sustaining high levels of inflammation.

Discussion

HIV infection primarily targets CD4+ T cells and restoring normal CD4+ T counts has consistently been a key indicator of successful immune reconstitution in PLWH [40,41]. Nevertheless, HIV also impacts other immune cells, including CD8+ T cells, which are crucial for controlling viral replication [42,43]. Despite this, the expanded pool of CD8+ T cells does not appear to significantly enhance viral control but instead contributes to inflammaging and adverse events in PLWH [13,44,45]. In this study, we applied bulk TCR sequencing to illustrate the changes in T cell clonal expansion across different stages of HIV infection. We found that PLWH, even after long-term ART, exhibit high level of T-cell clonal expansion, which is associated with the treatment duration, virological response, and immune reconstitution. Furthermore, by integrating single-cell RNA with TCR sequencing, we identified GNLY+CD8+ T cells as the subpopulation responsible for clonal expansion and maintenance in PLWH. We elucidated the characteristics of GNLY+CD8+ T cells, including low exhaustion, high cytotoxicity, and predominant expression of the pro-inflammatory 15 kDa GNLY isoform. Additionally, IL-15 significantly stimulated their expansion and activation. Functional experiments demonstrated that degranulated CD8+ T cells activate monocytes to secrete inflammatory factors and disrupt the integrity of intestinal epithelial cells through the release of GNLY. These findings highlight GNLY+CD8+ T cells as a critical population driving abnormal CD8+ T-cell clonal expansion and a potential contributor to inflammaging in PLWH.

Aging is a complex and multifactorial process of physiological changes strongly associated with various human diseases. A growing number of studies have comprehensively explored the molecular changes that occur during aging using omics profiling to build “aging clocks’, such as epigenomic clocks, inflammatory clocks and gut microbiome clocks [26,39,46]. In light of this, PLWH exhibit accelerated biological aging as measured by epigenetic aging clocks compared to HC [47,48]. The human TCR repertoire changes with age [27], and has also been used to model a TCR clock [26]. In this study, we defined indices reflecting T-cell clonal expansion, and modeled the age-related trends by these TCR indices for HC and PLWH, respectively. We found that HC exhibit nonlinear patterns of aging, with substantial dysregulation occurring at approximately 33 years and 55 years of chronological age. The nonlinear patterns of aging by TCR indices align with the results of a recent multi-omics study [28]. However, we found that the specific nodes occur earlier than the results from multi-omics. We hypothesize that human aging is not synchronized across different omics layers, exhibiting a spatiotemporal order in which TCR aging occurs earlier than other omics, such as proteomics. In contrast, PLWH showed a linear pattern of accelerated aging, with a start below the plateau stage in HC aged 30–55 as early as in their twenties. These findings indicate that clonally expanded T cells are closely associated with the accelerated aging observed in PLWH. Unlike similar life expectancy between PLWH and HC, premature aging reflected by TCR repertoire may highlight the disparity in overall health in PLWH. However, due to the limitations of bulk TCR sequencing data, we cannot accurately distinguish the contributions of CD4+ T cells and CD8+ T cells to these phenomena. Based on previous reports [49], the clonal expansion of CD8+ T cells significantly increases in the elderly population and is considered a key marker of immune aging. We hypothesize that the premature aging trend observed in our study may primarily be driven by CD8 + T cells. Analyzing and modeling purified CD4 + and CD8+ T cells separately would likely yield more definitive results in the future.

The phenotypic characteristics of GNLY+CD8+ T cells are consistent at the transcriptomic and protein level. Despite exhibiting senescence, these clonal cells displayed high cytotoxicity and low exhaustion. Although we were not able to dissect whether the clonally expanded cells were explicitly responsive to antigens such as HIV, CMV, or EBV, it has been reported that this oligoclonal T-cell expansion in PLWH is not specific to any of these antigens [9]. In addition, the de novo NK cell receptors and the downregulation of its co-stimulatory molecules make this group of cells acquire the activation pathway of innate TCR-independent response [50,51], which may also be responsible for impaired specific antiviral immunity in vivo and proliferation of CD8+ T cell clonal expansions in vitro [52]. Recent reports have found that chronic antigen stimulation may induce changes in the CD8+ T-cell receptor repertoire, leading to the expression of NK cell receptors, which are more sensitive to bystander activation through innate cytokines, including IL-12, IL-18 and IL-15 [53–55]. The type and density of NK cell receptors and other phenotypic changes confer strong functional heterogeneity in these cells. Their roles range from providing immune protection in long-lived elderly individuals to contributing to immunosuppression and immune escape in cancer patients. Thus, these clonal CD8+ T cells may have undergone a state transition from TCR-dependent to

TCR-independent stimulation and still retain crucial effector function. In our study, the enhancement of bystander activation signaling pathways in GNLY +CD8+ T cells after ART, combined with high expression of cytokine receptors, elevated plasma cytokine levels, and the significant induction of GNLY +CD8+ T-cell expansion and activation by IL-15 in vitro, highlights the critical role of bystander activation in the clonal maintenance and expansion of these cells.

HIV infection disrupts the intestinal epithelial barrier [56,57], increasing gut permeability to microorganisms and their products [58]. This enhanced permeability can lead to local and systemic inflammation. However, long-term ART is unable to repair the damage to the gut's epithelial barrier caused by HIV, resulting in ongoing microbial translocation and inflammation. Functional experiments demonstrated that the supernatant of IL-15-stimulated CD8 + T cells significantly activates monocytes to secrete inflammatory factors and disrupts the integrity of intestinal epithelial cells. Furthermore, anti-GNLY antibodies effectively alleviate these effects, indicating that GNLY derived from CD8+ T cells plays a critical role in sustaining high levels of inflammation and intestinal barrier damage in PLWH. Collectively, our findings demonstrate that GNLY+CD8+ T cells, enhanced by bystander activation pathways, are the primary cell population responsible for clonal expansion and maintenance highlighting these cells as a significant contributor to exacerbating inflammaging for PLWH.

In summary, we delineated the dynamic perturbations of the TCR repertoire at different stages of HIV infection, characterized by significant clonal expansion, which is associated with clinical prognosis and premature aging in PLWH. Further analysis identified GNLY+CD8+ T cells as the primary population undergoing continuous clonal expansion both before and after ART, with a critical role in promoting inflammation and disrupting the intestinal barrier. Our study highlights new research directions for a deeper understanding of inflammaging in HIV infection.

Acknowledgments

We thank Chunbao Zhou, Jinhong Yuan and Huiwei Sun (Chinese PLA General Hospital) for technical assistance with FACS. We thank Songshan Wang, Zhijie Wang and Jiaying Li (Chinese PLA General Hospital) for technical assistance with immunofluorescence. We thank the sequencing platform of the Chengdu ExAb Biotechnology Ltd. We thank all the patients for their contributions to the study.

Disclosure statement

Dr. Zhixi Zhang is the founder of Chengdu ExAb Biotechnology Ltd. All financial interests are unrelated to this study. The remaining authors declare no competing interests.

Funding

This work was supported by [National Natural Science Foundation of China #1] under Grant 82270629; [National Natural Science Foundation of China #2] under Grant 82100177; [National Natural Science Foundation of China #3] under Grant 82271781; [Clinical Medical Scientist Project of Henan Province, China #4] under Grant 2024-06; [Henan Provincial Science Fund for Distinguished Young Scholars, China #5] under Grant 232300421011; [Program for Science & Technology Innovation Talents in Universities of Henan Province, China #6] under Grant 24HASTIT064; [Young and Middle-aged Academic Leaders of Health Commission of Henan Province, China #7] under Grant HNSWJW-2023029; [Funding for Scientific Research and Innovation Team of The First Affiliated Hospital of Zhengzhou University, China #8] under Grant QNCXTD2023014.

Author contributions

Q-LZ, F-SW, Z-XZ and J-YZ conceived and supervised this study; H-FW, L-PZ, and LZ collected clinical samples and performed the experiments; CZ and S-YC led the bioinformatic analyses; H-FW, W-ZL, B-PY, M-JZ, Q-XG, XL, B-LY and FS collected clinical information; H-HH provided experimental samples; H-FW, CZ and J-YZ analyzed the data and wrote the manuscript. All authors read and approved the final manuscript.

Institutional review board statement

The study was conducted in accordance with the Declaration of Helsinki, and approved by the Research Ethics Committee of the Fifth Medical Center of the PLA General Hospital (protocol code ky-2021-7-6-1 and approved on 20 July 2021).

References

[1] Wang FS, Zhang L, Douek D, et al. Strategies for an HIV cure: progress and challenges. Nat Immunol. 2018;19(11):1155–1158. doi:10.1038/s41590-018-0242-8

[2] Wang XM, Zhang JY, Xing X, et al. Global transcriptomic characterization of T cells in individuals with chronic HIV-1 infection. Cell Discov. 2022;8(1):29. doi:10.1038/s41421-021-00367-x

[3] Marcus JL, Leyden WA, Alexeeff SE, et al. Comparison of overall and comorbidity-free life expectancy between insured adults with and without HIV infection, 2000-2016. JAMA Netw Open. 2020;3(6):e207954. doi:10.1001/jamanetworkopen.2020.7954

[4] Franceschi C, Campisi J. Chronic inflammation (inflammaging) and its potential contribution to age-associated diseases. J Gerontol A Biol Sci Med Sci. 2014;69(Suppl 1):S4–S9. doi:10.1093/gerona/glu057

[5] Franceschi C, Garagnani P, Parini P, et al. Inflammaging: a new immune-metabolic viewpoint for age-related diseases. Nat Rev Endocrinol. 2018;14(10):576–590. doi:10.1038/s41574-018-0059-4

[6] Sieg SF, Shive CL, Panigrahi S, et al. Probing the Interface of HIV and Inflammaging. Curr HIV/AIDS Rep. 2021;18(3):198–210. doi:10.1007/s11904-021-00547-0

[7] Zhang C, Song JW, Huang HH, et al. NLRP3 inflammasome induces CD4+ T cell loss in chronically HIV-1-infected patients. J Clin Invest 2021;131(6):e138861. doi:10.1172/jci138861
[8] Towlerton AMH, Ravishankar S, Coffey DG, et al. Serial analysis of the T-cell receptor beta-chain repertoire in people living with HIV reveals incomplete recovery after long-term antiretroviral therapy. Front Immunol. 2022;13:879190. doi:10.3389/fimmu.2022.879190
[9] Turner CT, Brown J, Shaw E, et al. Persistent T cell repertoire perturbation and T cell activation in HIV after long term treatment. Front Immunol. 2021;12:634489. doi:10.3389/fimmu.2021.634489
[10] Younes S-A, Freeman ML, Mudd JC, et al. IL-15 promotes activation and expansion of CD8+ T cells in HIV-1 infection. J Clin Invest 2016;126(7):2745-2756. doi:10.1172/JCI85996
[11] Helleberg KGM, Ullum H, Ryder LP, et al. Course and clinical significance of CD8+ T-cell counts in a large cohort of HIV-infected individuals. J Infect Dis. 2015;211(11):1726–1734.
[12] Liu J, Wang L, Hou Y, et al. Immune restoration in HIV-1-infected patients after 12 years of antiretroviral therapy: a real-world observational study. Emerg Microbes Infect. 2020;9(1):2550–2561. doi:10.1080/22221751.2020.1840928
[13] Mussini C, Lorenzini P, Cozzi-Lepri A, et al. CD4/CD8 ratio normalisation and non-AIDS-related events in individuals with HIV who achieve viral load suppression with antiretroviral therapy: an observational cohort study. Lancet HIV. 2015;2(3):e98–106. doi:10.1016/S2352-3018(15)00006-5
[14] Serrano-Villar S, Deeks SG. CD4/CD8 ratio: an emerging biomarker for HIV. Lancet HIV 2015;2(3):e76–e77. doi:10.1016/S2352-3018(15)00018-1
[15] Sainz T, Serrano-Villar S, Díaz L, et al. The CD4/CD8 ratio as a marker T-cell activation, senescence and activation/exhaustion in treated HIV-infected children and young adults. AIDS. 2013;27(9):1513–1516. doi:10.1097/QAD.0b013e32835faa72
[16] Ron R, Moreno E, Martinez-Sanz J, et al. CD4/CD8 Ratio During Human Immunodeficiency Virus Treatment: Time for Routine Monitoring? Clin Infect Dis. 2023;76(9):1688–1696. doi:10.1093/cid/ciad136
[17] Wan LY, Huang HH, Zhen C, et al. Distinct inflammation-related proteins associated with T cell immune recovery during chronic HIV-1 infection. Emerg Microbes Infect. 2023;12(1):2150566. doi:10.1080/22221751.2022.2150566
[18] Bektas A, Schurman SH, Sen R, et al. Human T cell immunosenescence and inflammation in aging. J Leukocyte Biol. 2017;102(4):977–988. doi:10.1189/jlb.3RI0716-335R
[19] Lu J, Ahmad R, Nguyen T, et al. Heterogeneity and transcriptome changes of human CD8+ T cells across nine decades of life. Nat Commun. 2022;13(1):5128. doi:10.1038/s41467-022-32869-x
[20] Jonsson AH, Zhang F, Dunlap G, et al. Granzyme K(+) CD8 T cells form a core population in inflamed human tissue. Sci Transl Med 2022;14(649):eabo0686. doi:10.1126/scitranslmed.abo0686
[21] Yu W, Li C, Zhang D, et al. Advances in T cells based on inflammation in metabolic diseases. Cells 2022;11(22):3554. doi:10.3390/cells11223554
[22] Zhang J-Y. Activation-induced pyroptosis contributes to the loss of MAIT cells in chronic HIV-1infected patients. 2022.
[23] Zhuo Y, Yang X, Shuai P, et al. Evaluation and comparison of adaptive immunity through analyzing the diversities and clonalities of T-cell receptor repertoires in the peripheral blood. Front Immunol. 2022;13:916430. doi:10.3389/fimmu.2022.916430
[24] Chiffelle J, Genolet R, Perez MA, et al. T-cell repertoire analysis and metrics of diversity and clonality. Curr Opin Biotechnol. 2020;65:284–295. doi:10.1016/j.copbio.2020.07.010
[25] Hou D, Ying T, Wang L, et al. Immune repertoire diversity correlated with mortality in avian influenza A (H7N9) virus infected patients. Sci Rep. 2016;6:33843. doi:10.1038/srep33843
[26] Hu J, Pan M, Reid B, et al. Quantifiable blood TCR repertoire components associate with immune aging. Nat Commun. 2024;15(1):8171. doi:10.1038/s41467-024-52522-z
[27] Sun X, Nguyen T, Achour A, et al. Longitudinal analysis reveals age-related changes in the T cell receptor repertoire of human T cell subsets. J Clin Invest 2022;132(17):e158122. doi:10.1172/JCI158122
[28] Shen X, Wang C, Zhou X, et al. Nonlinear dynamics of multi-omics profiles during human aging. Nat Aging 2024;4(11):1619–1634. doi:10.1038/s43587-024-00692-2
[29] Li J, Xiong M, Fu X-H, et al. Determining a multimodal aging clock in a cohort of Chinese women. Med 2023;4(11):825–848.e13. doi:10.1016/j.medj.2023.06.010
[30] Pai JA, Hellmann MD, Sauter JL, et al. Lineage tracing reveals clonal progenitors and long-term persistence of tumor-specific T cells during immune checkpoint blockade. Cancer Cell 2023;41(4):776–790.e7. doi:10.1016/j.ccell.2023.03.009
[31] Miron M, Meng W, Rosenfeld AM, et al. Maintenance of the human memory T cell repertoire by subset and tissue site. Genome Med. 2021;13(1):100. doi:10.1186/s13073-021-00918-7
[32] Zheng L, Qin S, Si W, et al. Pan-cancer single-cell landscape of tumor-infiltrating T cells. Science (New York, NY). 2021;374(6574):abe6474. doi:10.1126/science.abe6474
[33] Peña SV, Hanson DA, Carr BA, et al. Processing, subcellular localization, and function of 519 (granulysin), a human late T cell activation molecule with homology to small, lytic, granule proteins. J Immunol. 1997;158(6):2680–2688.
[34] Clayberger C, Finn MW, Wang T, et al. 15 kDa granulysin causes differentiation of monocytes to dendritic cells but lacks cytotoxic activity. J Immunol. 2012;188(12):6119–6126. doi:10.4049/jimmunol.1200570
[35] Sparrow E, Bodman-Smith MD. Granulysin: The attractive side of a natural born killer. Immunol Lett. 2020;217:126–132. doi:10.1016/j.imlet.2019.11.005
[36] Dotiwala F, Lieberman J. Granulysin: killer lymphocyte safeguard against microbes. Curr Opin Immunol. 2019;60:19–29. doi:10.1016/j.coi.2019.04.013
[37] Crespo ÂC, Mulik S, Dotiwala F, et al. Decidual NK cells transfer granulysin to selectively kill bacteria in trophoblasts. Cell 2020;182(5):1125–1139.e18. doi:10.1016/j.cell.2020.07.019
[38] Lettau M, Dietz M, Dohmen K, et al. Granulysin species segregate to different lysosome-related effector

vesicles (LREV) and get mobilized by either classical or non-classical degranulation. Mol Immunol. 2019;107:44–53. doi:10.1016/j.molimm.2018.12.031
[39] Singh S, Giron LB, Shaikh MW, et al. Distinct intestinal microbial signatures linked to accelerated systemic and intestinal biological aging. Microbiome. 2024;12(1):31. doi:10.1186/s40168-024-01758-4
[40] Yang X, Su B, Zhang X, et al. Incomplete immune reconstitution in HIV/AIDS patients on antiretroviral therapy: Challenges of immunological non-responders. J Leukoc Biol. 2020;107(4):597–612. doi:10.1002/JLB.4MR1019-189R
[41] Espineira S, Flores-Piñas M, Chafino S, et al. Multi-omics in HIV: searching insights to understand immunological non-response in PLHIV. Front Immunol. 2023;14:1228795. doi:10.3389/fimmu.2023.1228795
[42] Collins DR, Gaiha GD, Walker BD. CD8+ T cells in HIV control, cure and prevention. Nat Rev Immunol. 2020;20(8):471–482. doi:10.1038/s41577-020-0274-9
[43] Bekker L-G, Beyrer C, Mgodi N, et al. HIV infection. Nat Rev Dis Primers. 2023;9(1):42. doi:10.1038/s41572-023-00452-3
[44] Trickey A, May MT, Schommers P, et al. CD4:CD8 ratio and CD8 count as prognostic markers for mortality in human immunodeficiency virus–infected patients on antiretroviral therapy: the antiretroviral therapy cohort collaboration (ART-CC). Clin Infect Dis. 2017;65(6):959–966. doi:10.1093/cid/cix466
[45] Luz Correa B, Ornaghi AP, Cerutti Muller G, et al. The inverted CD4:CD8 ratio is associated with cytomegalovirus, poor cognitive and functional states in older adults. Neuroimmunomodulation. 2014;21(4):206–212. doi:10.1159/000356827
[46] Horvath S. DNA methylation age of human tissues and cell types. Genome Biol. 2013;14(10):R115.
[47] Mikaeloff F, Gelpi M, Escos A, et al. Transcriptomics age acceleration in prolonged treated HIV infection. Aging Cell. 2023;22(10):e13951. doi:10.1111/acel.13951
[48] Breen EC, Sehl ME, Shih R, et al. Accelerated aging with HIV begins at the time of initial HIV infection. iScience 2022;25(7):104488. doi:10.1016/j.isci.2022.104488
[49] Mogilenko DA, Shpynov O, Andhey PS, et al. Comprehensive profiling of an aging immune system reveals clonal GZMK+ CD8+ T cells as conserved hallmark of inflammaging. Immunity. 2021;54(1):99–115.e12. doi:10.1016/j.immuni.2020.11.005
[50] Jin JH, Huang HH, Zhou MJ, et al. Virtual memory CD8+ T cells restrain the viral reservoir in HIV-1-infected patients with antiretroviral therapy through derepressing KIR-mediated inhibition. Cell Mol Immunol. 2020;17(12):1257–1265. doi:10.1038/s41423-020-0408-9
[51] Yang X, Zhen C, Huang H, et al. Implications of Accumulation of Clonally Expanded and Senescent CD4 + GNLY+ T Cells in Immunological Non-responders of HIV-1 infection. Emerging Microbes Infect. 2024;13(1):2396868. doi:10.1080/22221751.2024.2396868
[52] Messaoudi I, Lemaoult J, Guevara-Patino JA, et al. Age-related CD8 T cell clonal expansions constrict CD8 T cell repertoire and have the potential to impair immune defense. J Exp Med. 2004;200(10):1347–1358. doi:10.1084/jem.20040437
[53] Roy Chowdhury R, Valainis JR, Dubey M, et al. NK-like CD8+ γδ T cells are expanded in persistent Mycobacterium tuberculosis infection. Science Immunology. 2023;8(81):eade3525. doi:10.1126/sciimmunol.ade3525
[54] Gehring AJ, MacParland SA. Intrahepatic T cells with NK-like properties: expanding the repertoire of lymphocytes sensitive to bystander activation. J Hepatol 2022;77(4):915–917. doi:10.1016/j.jhep.2022.08.001
[55] Pita-López ML, Pera A, Solana R. Adaptive memory of human NK-like CD8+ T-cells to aging, and viral and tumor antigens. Front Immunol. 2016;7:616. doi:10.3389/fimmu.2016.00616
[56] Niessen CM. Tight junctions/adherens junctions: basic structure and function. J Invest Dermatol. 2007;127(11):2525–2532.
[57] Wang Z, Zhen C, Guo X, et al. Landscape of gut mucosal immune cells showed gap of follicular or memory B cells into plasma cells in immunological non-responders. Clin Transl Med. 2024;14(5):e1699. doi:10.1002/ctm2.1699
[58] Brenchley JM, Price DA, Schacker TW, et al. Microbial translocation is a cause of systemic immune activation in chronic HIV infection. Nat Med. 2006;12(12):1365–1371.